Biofabrication and Characterization of Zinc Oxide Nanoparticles Using *Staphylococcus aureus*

Venus D. Najeeb[1†], Fattma A. Ali[2] and Sameira S. Swilaiman[1]

[1]Department of Basic Science, College of Dentistry, Hawler Medical University, Kurdistan Region – F.R. Iraq
[2]Department of College of Health Science, Hawler Medical University, Kurdistan Region – F.R. Iraq

***Abstract*—Due to their large surface area and catalytic properties, zinc oxide nanoparticles (ZnO-NPs) are highly effective in biological applications. In this study, ZnO-NPs were biofabricated using the American Type Culture Collection *Staphylococcus aureus* (ATCC 25923) and characterized by double-beam ultraviolet-visible spectroscopy, with a characteristic absorption peak at 351 nm, verifying the synthesis of ZnO-NPs. Proteins and carboxyl and hydroxyl groups that function as reducing and stabilizing agents were found on the surface of biosynthesized ZnO-NPs, as revealed by Fourier transform infrared analysis. The hexagonal structure was validated by X-ray diffraction analysis. Spherical shape confirmed by Field Emission Scanning Electron Microscopy, and the main elements detected by energy-dispersive spectroscopy were Zinc 79.91% and oxygen 18.33%. Transmission electron microscopy investigation revealed that the ZnO-NPs produced were predominantly quasi-spherical to irregular shape, with diameters in the nanoscale range (approximately 40–60 nm). The results indicated that the diameter of inhibitory zones against methicillin-resistant *S. aureus* (MRSA) using varying concentrations of 50, 25, 12.5, 6.25, and 3.125 μg/mL of ZnO-NPs in an agar well diffusion test ranged from 7 to 24 mm, and the cytotoxicity of ZnO-NPs was assessed by MTT assay. Human embryonic kidney 293 cells were used. Our research demonstrates that biofabricated ZnO-NPs using standard *S. aureus* exhibit successful characterization and strong anti-MRSA activity, which may represent a promising path for the development of innovative antimicrobial agents, particularly for treating MRSA as multidrug-resistant isolates.**

***Index Terms*—American type culture collection 25923, Anti-methicillin-resistant *Staphylococcus aureus*, Characterization, Cytotoxicity, Zinc nanoparticles.**

I. Introduction

Nanoscience is an interdisciplinary field of science that emphasizes the development, design, and processing of nanoparticles (NPs) with sizes between 1 nm and 100 nm (Hamad, Chawsheen and Al-Naqshbandi, 2022) The use of bacteria, plants, fungi, or algae to produce NPs can serve as a nanofactory, developing innovations that are safe, non-toxic, inexpensive, and environmentally friendly for a variety of uses in the basic and applied sciences. Bacteria are commonly used in the manufacture of NPs since these substances are simple to handle and genetically manipulated (Haji, Ali and Aka, 2022). NPs have a high surface-to-volume ratio of atoms on the surface to atoms inside the material, compared to bulk materials and specific chemical and physical properties, such as electricity and magnetic properties and effective antibacterial agents for treatment of infectious diseases and a variety of applications in the biological and medical research (Alnuaimi, et al., 2022).

Metal oxides, such as zinc oxide, are important due to their stability, safety, and non-toxicity. Zinc oxide NPs (ZnO-NPs) are gaining popularity for their biological applications, including labeling in nanomedicine, medication administration, biological sensing, and gene delivery. Further, they have been shown to have antifungal, antibacterial, antidiabetic, and acaricidal abilities. ZnO-NPs exhibit varying antibacterial properties, which depend on their stability, size, and concentration inside the growth conditions. The mode of action of ZnO-NPs is still being studied. However, it is hypothesized that their antibacterial properties are mediated by the formation of hydrogen peroxide or the direct interaction of ZnO-NPs that attach to bacterial surfaces through electrostatic forces (Hayat, et al., 2022). Due to ZnO's properties to absorb and scatter ultraviolet (UV) light, it is used in personal care products, such as sunscreens and cosmetics. Zn is an essential trace element present in many body tissues and a cofactor of many enzymes; it plays a role in (Fakhari, Jamzad, and Kabiri Fard, 2019).

Multidrug-resistant (MDR) pathogens have become more prevalent as a consequence of the widespread use of broad-spectrum antibiotics in hospitals (Ali and Al-Jaff, 2021). Overuse of antibiotics has reduced their effectiveness as antimicrobial resistance has become widespread and is now life-threatening. Physicians and researchers have developed several therapeutic ways to address this challenge. *Staphylococcus aureus*, especially methicillin-resistant *S. aureus* (MRSA), is classified as a high-priority pathogen by the WHO because of its antibiotic resistance and capacity

ARO-The Scientific Journal of Koya University
Vol. XIV, No.1(2026), Article ID: ARO.12747. 9 pages
DOI: 10.14500/aro.12747
Received: 11 November 2025; Accepted: 17 January 2026
Regular research paper; Published: 10 April 2026
†Corresponding author's e-mail: venus.dilshad@hmu.edu.krd

to develop biofilms and produce a variety of virulence factors, including extracellular enzymes (e.g., coagulase A) and toxins (e.g., Panton-Valentine Leukocidin), which create biofilms, which pose a hazard to host tissues (e.g., bone and heart valves), medical implants and the food industry, contribute to disease progression, it is a Gram-positive human commensal that colonizes 80% of patients with nosocomial infections, as well as infections caused by antibiotic-resistant *S. aureus*, which cost the US healthcare system $1.7 billion annually and kill 11,000 persons (Rafael, et al., 2023). Numerous diseases, including infective endocarditis, infections of prosthetic devices, osteoarticular infections, bacteremia, pneumonia, and infections of the skin and soft tissues, have been linked to the commensal and opportunistic pathogen *S. aureus* (Omer, et al., 2024).

This study employed a quality control strain of *S. aureus*, (American Type Culture Collection [ATCC] 25923), as a precursor to synthesize ZnO-NPs, the structural, and optical characteristics of them were evaluated by UV–visible (UV–Vis) spectroscopy, Fourier-transform infrared spectroscopy (FTIR), X-ray diffraction (XRD), energy-dispersive spectroscopy (EDS) linked to field emission scanning electron microscopy (FESEM), and transmission electron microscopy (TEM) and the antibacterial activity against clinically isolated MDR and MRSA *S. aureus* strains, The *mec*A gene, which encodes the penicillin-binding protein 2a that confers β-lactam resistance, was genetically detected to verify the existence of MRSA. To evaluate the possible role of integrons in the spread of resistance genes among isolates, the integrase gene (*int1*), a marker of class 1 integrons linked to horizontal gene transfer) of resistance determinants was also targeted. To assess cell viability, human embryonic kidney 293 cells (HEK293) were employed using the MTT assay (3-(4,5-dimethylthiazol-2-yl)-2,5-diphenyltetrazolium bromide), which evaluates mitochondrial metabolic activity, indicating the viability of HEK293 cells after treatment. The MTT assay was used to assess cytotoxicity.

II. Materials and Methods

A. Biofabrication of ZnO-NPs

According to an official document from the College of Dentistry, Hawler Medical University, ATCC 25923 was acquired from Medya Diagnostic Centre, Erbil, as a quality control of *S. aureus* used for biofabrication. The first step was to prepare a stock solution of 4.39 g (0.02 mol) of Zinc acetate dihydrate $Zn(CH_3COO)_2 \cdot 2H_2O$ above a hotplate magnetic stirrer with 1000 mL of deionized water (pH 7) at 65°C for 10 min (Elabbasy, et al., 2025). After 3 days, *S. aureus* (ATCC 25923) was cultured in nutrient broth at 37°C in a shaking incubator set to 150 rpm. During subsequent incubation, the bacterial cell walls were disrupted by sonicating the growth (probe type) for 5 min in ice cubes around the flask. After centrifugation at 6000 rpm for 30 min, the sediment was disposed of, and the supernatant was collected. Using a 0.45 μm syringe filter, the bacterial supernatant (20 mL) was dropped into (980 mL) of the prepared stock solution, which was cooled to 30°C and stirred continuously. The pH was adjusted with a pH meter by adding drops of 4 M NaOH until white precipitates formed. After an hour of sonication, the colloidal solution was left at room temperature for 24 h. The sediment was centrifuged 3 times with deionized water for 20 min each and once with 90% ethanol. After 1 day of drying at 60°C, the white powder was split into two portions. One-half was preserved for further analysis (Hayat, et al., 2022; Abdo, et al., 2021).

B. ZnO-NPs Characterizations

White powder was frequently a result of ZnO-NPs production. The precipitation at the flask bottom was the first indicator of NP formation; using a double-beam (UV-vis) spectrophotometer became the second confirmation of nanostructures detection (PerkinElmer Lambda, USA), wavelength range for measuring peak was (200–800) nm. FTIR was used for examining the properties of the ZnO-NP functional groups. (JASCO Spectrum 4600). At a spatial resolution of 4 cm^{-1}, the NPs were analyzed in the 4000–450 cm^{-1} spectrum range. XRD measurements were performed using a PANalytical X'Pert PRO diffractometer applying Cu Kα (λ = 1.5406 Å) radiation to evaluate its chemical composition and crystal shape. The reflected intensity has been determined from 20° to 80° after the device was set to 40 mA and 40 kV. Powdered ZnO-NP samples were placed on the XRD grid, and the results were obtained using the Scherrer equation ($D = K\lambda/\beta \cos \theta$). The Debye Scherrer equation was applied to calculate the average size of the crystallite in each peak. TEM (Titan G2 60–300, FEI, USA): image and probe, FEI, USA) and Advanced FESEM (FEI Quanta 450 FEG) were employed to investigate the ZnO-NPs form and size of particle distribution. The sample was placed on a copper carbon-coated TEM grid and allowed to dry, resulting in a thin layer of film. The elemental composition of ZnO-NPs was investigated using (EDS) linked to FESEM.

C. Anti-MRSA Potency of ZnO-NPs

Bacterial sources

This study examined 172 samples (60% male and 40% female) from several infection sites in Rezgary. Nanakaly Hospitals in Erbil, Iraq's Kurdistan Region, between April and December 2024, the samples examined included urine (95), sputum (7), wound swabs (19), blood (7), upper vaginal swabs (23), seminal fluid (11), synovial fluid (3), ear swabs (3), throat swabs (2), and nasal swabs (2). The ethical committee of the College of Dentistry at Hawler Medical University approved this study. All isolates were verified as *S. aureus* phenotypically, biochemically, and genetically using culturing, and conventional PCR (polymerase chain reaction) to identify MRSA-associated genes (*mecA*) and (*Int1*) and confirm their resistance profile.

Lab-cultured bacteria and storage

Briefly, specimens were collected and inoculated separately onto blood agar and mannitol salt agar using a sterile loop, forming parallel lines on clean surfaces.

After aerobic incubation (24 h at 37°C), Catalase-positive colonies were examined for coagulase enzyme production by incubating 2–3 colonies with diluted plasma for 2–3 h. All positive strains were tested against nine antibiotics from different classes, including oxacillin, cefoxitin, levofloxacin, erythromycin, clindamycin, gentamicin, tetracycline, trimethoprim/sulfamethoxazole, vancomycin, and linezolid, using the automated Vitek-2 system version 9.02, bioMérieux S.A., France protocol VITEK®2 GP Reference 21342. (Al-Naqshbandi, et al., 2021). Pure colonies were stored in Eppendorf tubes containing 600 µL of brain heart infusion and 400 µL of glycerol at −20°C, as described by (El-Masry, et al., 2022).

Molecular study

To select the most pathogenic bacterial strains, the detection of the *mecA and Int1* genes was genetically confirmed using PCR. Genomic DNA was extracted from bacterial culture utilizing the Beta Bayen tissue and bacterial DNA preparation kit (Beta Bayen GmbH, 90453 Bayen, Germany), Table I.

Anti-MRSA activity of ZnO-NPs

ZnO-NPs were tested for antibacterial activity against MRSA strains (including *mecA and Int1* genes), using an agar well diffusion method at five different doses (50, 25, 12.5, 6.25, and 3.125 µg/mL). Briefly, an 18-h-old culture of *S. aureus* strains were cultivated on nutrient agar at 37°C and then, using a spectrophotometer, standardized to a 0.5 McFarland turbidity standard (roughly 1.5×10^8 CFU/mL) to obtain an optical density (OD600) of 0.08–0.09 to guarantee a constant inoculum density throughout all experiments to obtain a uniform bacterial lawn, a sterile cotton swab was used to spread the cell solution on Mueller-Hinton agar. Plates were allowed to dry before making 6mm-diameter wells with a sterile cork borer. Pipette 70 µL of each concentration into each well, wait 15 min, then incubate at 37°C for 18 h. The diameter of the inhibition zone (IZ) was measured in mm, as described in a previous study (Haji, Ali, and Aka, 2022).

D. In vitro Cytotoxicity of ZnO-NPs

For cell viability checking, HEK293 were used. (3-(4,5-dimethylthiazol-2-yl)-2,5-diphenyltetrazolium bromide (MTT assay), a colorimetric test. The solvents required were Dimethyl Sulfoxide (DMSO)/acidified isopropanol. A Titertek Multiskan plate reader (ELISA reader) equipped with a fixed wavelength filter was used to measure optical density. A 600 nm filter was utilized throughout the studies, but a 550 nm filter was later purchased. The optical density of formazan solutions was measured using glass cuvettes on a spectrophotometer. All plate reader measurements were performed on samples stored in a 96-well multiplate. Each well of a 96-well plate was filled with HEK-293 cells (1×10^5 cells/well), followed by treatment with different concentrations of ZnO-NPs µl (5–500 µg/mL), increasing in concentration. A 5 mg/mL MTT solution in PSB was used subsequently. Each well was filled with 5 mg/mL of a solution of MTT in PBS (phosphate-buffered saline), sterilized by filtration, and then incubated for 4–6 h at 37°C. Before the formation of formazan particles, 200 µL of DMSO was added to each well to dissolve the particles, and the plate was agitated for 5 min. After the purple color was generated, the sample was examined for OD, and the results were recorded. Similar to Belteky, these variables were intentionally altered in some investigations (Belteky, et al., 2021).

E. Statistical Analysis

Data in comparison tests for inhibition tests were expressed as mean ± Standard Error of the Mean using the Statistical Package for the Social Sciences software. Heatmap and dendrogram analysis for similarity were performed using Origin 8 software. GraphPad version 9 was used for particle size distribution analysis.

III. Results and Discussion

A. Results

Biofabrication of ZnO-NPs

In this study, adding the cell-free supernatant of ATCC 25923 to an aqueous Zn^{2+} solution and after checking different pH finally at pH 12 resulted in the resulted in the reduction of Zn^{2+} ions to ZnO NPs, as indicated in Fig. 1. Visual inspection of the reaction mixture, comprising a bacterial suspension and Zn^{2+}, provided initial synthesis of ZnO-NPs formation, as white precipitates that were deposited at the bottom of flasks served as an indicator of this.

ZnO-NPs characterizations

For further characterization, the ZnO-NPs were dispersed in deionized water (dH_2O). UV-vis spectroscopy of the colloidal solution in the 200–800 nm range was used to monitor the reduction of Zn^{2+} to ZnO NPs. The formation of ZnO-NPs was confirmed by the UV-Vis spectrum of the ZnO-NPs sample, which displayed a deep peak at 351 nm, as shown in Fig. 2a. The results of FTIR spectroscopy for the composition of bioactive molecules in ZnO-NPs were used to evaluate the stretching vibrations of Zn–O bonds, which were confirmed by the distinctive peaks at 618.95 cm^{-1} and 471 cm^{-1}, indicating the successful formation of ZnO NPs,

TABLE I
Primers used in this Research

Gene	Oligonucleotide	Amplicon size (bp)	PCR profile temperature	References
mecA-F	AAAAAAGGTGGTATCGATTGGC	533	95° for 5 min; 95° for 38 s; 60° for 40 s;	(Wei, et al., 2023)
mecA-R	AGTTCTGCAGTACCGGATTTGC		72° for 1 min; 72° for 10 min; 4°∞	
Int1-F	GGTGTGGCGGGCTTCGTG	480	95° for 5 min; 95° for 38 s; 60° for 40 s;	(Mohemmad, et al., 2023)
Int1-R	GCATCCTCGGTTTTCTGG		72° for 1 min; 72° for 10 min; 4°∞	

http://dx.doi.org/10.14500/aro.12747

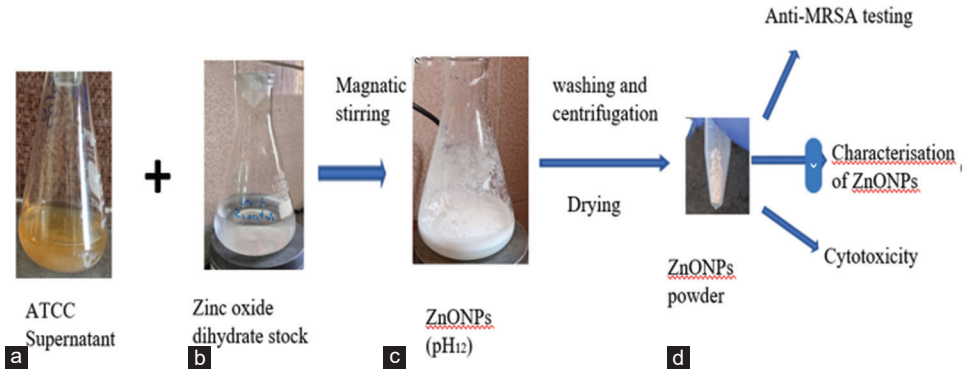

Fig. 1. Cell-free supernatant of American Type Culture Collection 25923 (a) was reduced Zn^{2+} (b) to zinc oxide nanoparticles (ZnO-NPs) (c). To produce a white, powdery substance of ZnO-NPs was repeatedly washed with distilled water, then ethanol, and ultimately dried overnight at 60°C (d).

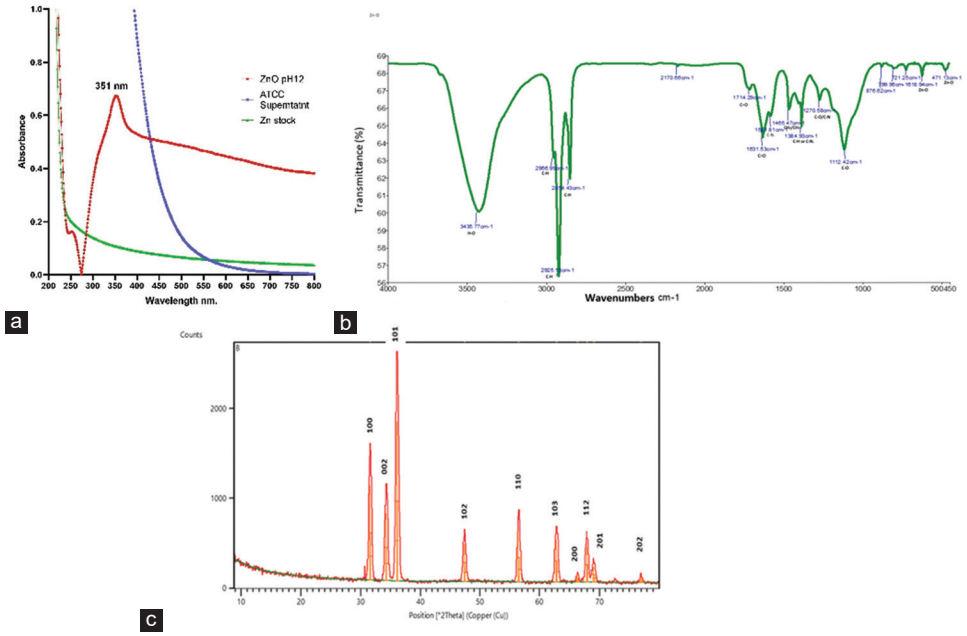

Fig. 2. In the wavelength range of 200–800 nm, the ultraviolet-visible spectrum of zinc oxide nanoparticles (ZnO-NPs) showed an absorption peak at 351 nm (red), American Type Culture Collection (ATCC 25923 supernatant (blue), and zinc oxide dihydrate stock (green). The inset image depicts biosynthesized ZnO-NPs dispersed in deionized water (a). Fourier-transform infrared spectra of ZnO-NPs biofabricated by ATCC (25923) (b). X-ray diffraction pattern recorded in the 2θ range of 20°–80°, these diffraction peaks confirm the hexagonal wurtzite crystal structure of ZnO nanoparticles (c).

which confirming the formation of ZnO NPs and were also supported by the results of the FTIR absorption spectra, a broad absorption peak at 3435.77 cm^{-1} indicated the presence of the O–H band, or hydroxyl functional group Fig. 2b. The result of XRD diffraction peaks, recorded in the 2θ range of 10–80° shoes hexagonal wurtzite ZnO, the (100), (002), (101), (102), (110), (103), (200), (112), (201), and (202) planes were represented by the diffraction peaks seen at 31.591°, 34.285°, 36.105°, 47.435°, 56.522°, 62.843°, 66.355°, 67.932°, 69.081°, and 77.015°, respectively, and the crystal size ranged between (16 and 17) nanometers, Fig. 2c. The altered nanofilm's surface morphology was analyzed by FE-SEM, revealing ZnO-NPs with irregular, quasi-spherical shapes. Despite a highly dispersed, re-aggregated distribution, the average size of NPs was determined to be 74.7 ± 22.4 nm. ZnO-NPs were verified to be present on the surface by EDX, which showed characteristic elemental peaks that indicated the composition. The ZnO-NPs have a highly crystallized structure with sharp vertices. That increased surface area led to an enhancement of their antibacterial characteristics, Fig. 3a-f.

Antibacterial study of ZnO-NPs

After phenotypic, biochemic, and genotypic laboratory identification of samples, the number of *S. aureus* was minimized to 47, 15, and 13 strains of MRSA, respectively, as shown in Fig. 4a-c.

MRSA-positive strains were used to test the antibacterial activity of ZnO-NPs at different concentrations. All of the tested microorganisms were affected by the NPs. NP size is a crucial factor in determining its antimicrobial potential, as it could easily enter cells. The measured IZ diameters of (50, 25, and 12.5) μg/mL against the MRSA strain (A) showed IZs of 21.67 ± 1.53 mm, 17.00 ± 1.00 mm, and 12.33 ± 3.21 mm;d however, at lower dosages (6.25 and 3.125 μg/mL), no IZ was

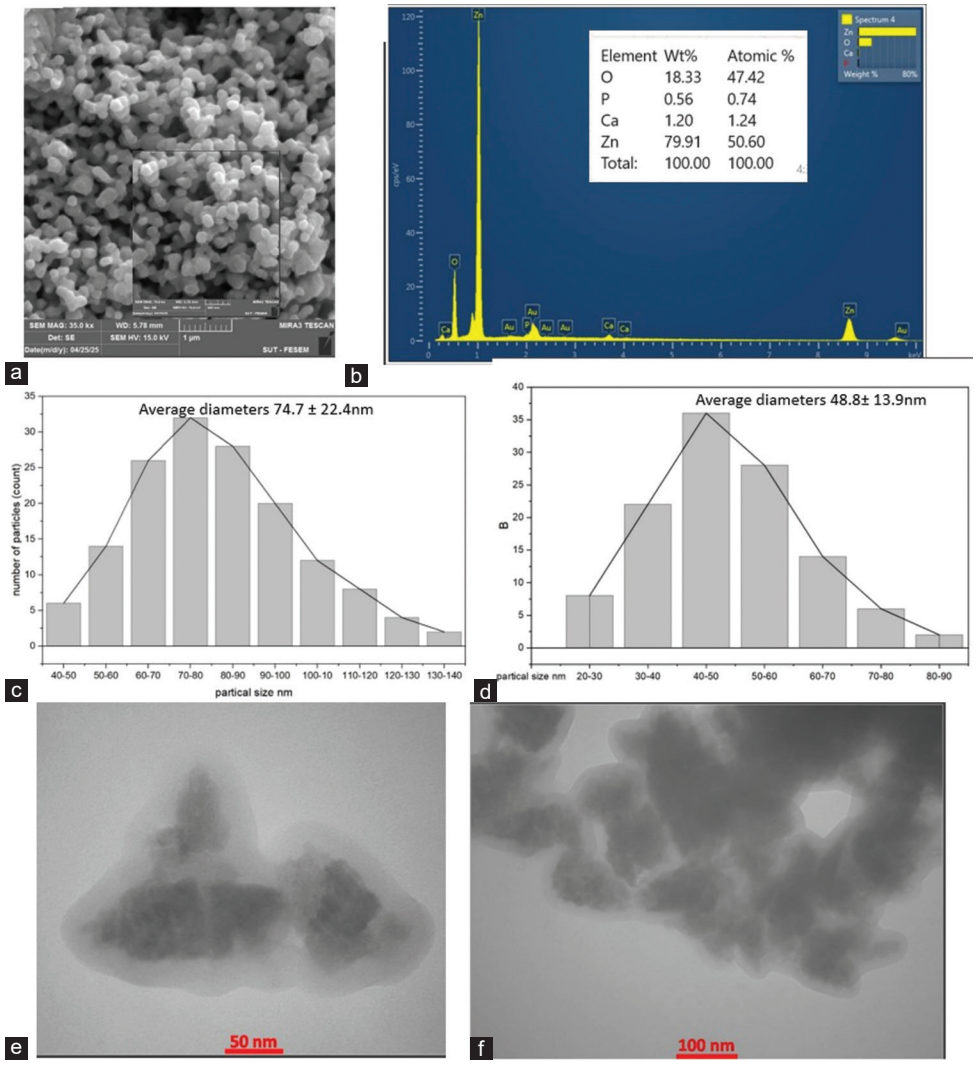

Fig. 3. Data collected from field emission scanning electron microscopy (FESEM) with energy dispersive X-ray analysis examinations of a good crystalline structure of biofabricated zinc oxide nanoparticles (ZnO-NPs) (a), and a highly pure ZnO (b). The average size of ZnO-NPs was shown in the distribution histogram FESEM (c), transmission electron microscopy (TEM) (d). TEM of ZnO-NPs (e and f).

observed. At 50, 25, 12.5, 6.25, and 3.125 µg/mL, the VRSA strain (B) exhibited smaller IZ diameters of 12.67 ± 1.53 mm, 10.67 ± 2.52 mm, 9.00 ± 1.73 mm, 4.67 ± 4.04 mm, and 0.00 mm. The sensitive ATCC 25923 strain exhibited the greatest response at the same doses, with IZ diameters of 23.83 ± 0.29, 21.00 ± 1.10, 15.00 ± 1.10, 13.67 ± 0.29, and 10.00 ± 0.29 mm, respectively. In the current study, ZnO-NPs biosynthesized by ATCC 25923 had a broad antibacterial spectrum as shown in Fig. 5. The results of IZ diameters by agar well diffusion showed remarkable inhibition effect of ZnO-NPs on all strains at concentration 50 and 25 µg/mL, except (C and 47) strains at concentration 12.5 µg/mL, (A, C, I, L, V, 11, 18, 45, and 47) strains at concentration 6.25 µg/mL, and all pathogenic strains were resistance at concentration 3.125 µg/mL of ZnO-NPs only ATCC 25923 strain was sensitive high significant differences between (Honest Significant Difference [HSD]) $p < 0.001$, with HSD between ATCC 25923 and all other strains except MRSA strain (A) at 50 µg/mL, (A, D, Y, and 3) at 12.5 µg/mL, and (D and 3) strains at 6.25 µg/mL when compared with a control (ATCC 25923), which was non-significant results, but HSD at 3.125 µg/mL as shown in Fig. 6a-e.

ZnO-NPs cytotoxicity results

The cytotoxicity of different doses of ZnO-NPs (0, 10, 25, 50, 100, 250, 500, 1000 µg/mL), after 6 h of incubation, with HEK293 was checked, which showed a decreased number of viable cells (%) by increasing of concentration of nano as done by MTT assays, which proven that the ZnO-NPs were cytotoxic to HEK293 and the IC_{50} measured as 14.8 µg/mL Fig. 7.

B. Discussion

As an alternative to chemical and physical methods, the use of microorganism NP synthesis has garnered considerable attention in recent years. Using the microorganism's biological materials, costly and harsh chemicals were eliminated. Extracellular or intracellular biological compounds from microorganisms can be used in the synthesis process of NPs. Successful biofabrication

http://dx.doi.org/10.14500/aro.12747

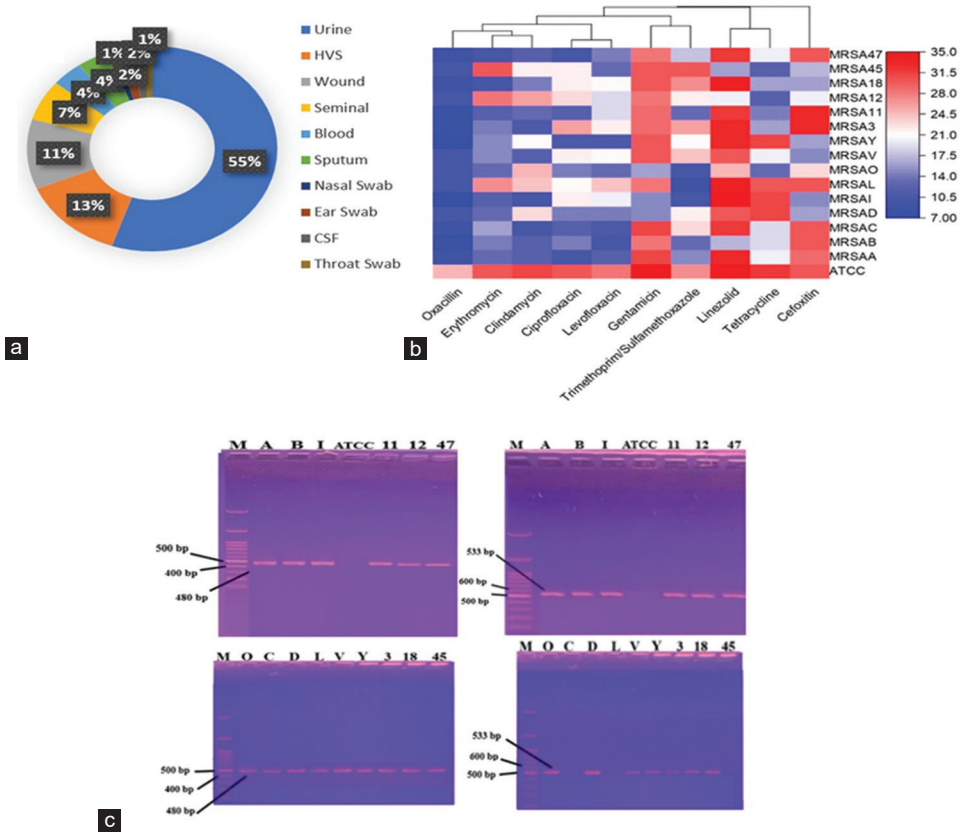

Fig. 4. (a-c) The distribution of clinical samples and the percentage of samples collected from patients are shown in the pie chart. Wounds had the highest percentage (33.3%), followed by urine (27.1%), blood (8.3%), high vaginal swabs (6.2%), seminal fluid (6%), sputum (4.2%), nasal swabs (4.2%), and each ear swab, throat swab, and cerebrospinal fluid at 2.1%. A heatmap with a color gradient, combined with a dendogram of similarity, by using oxacillin as an antibiotic, where all methicillin-resistant *Staphylococcus aureus* (MRSA) were resistant, whereas only American Type Culture Collection (ATCC) 25923 was sensitive, where higher resistance levels were red and lower resistances were blue, was used to illustrate how similar MRSA strains (rows) differed in their resistance to various antibiotics (columns). Both genes (*mecA*, 533 bp, and Int1, 480 bp) were detected by agarose gel electrophoresis of the polymerase chain reaction-amplified products. M: marker, ATCC 25923 as control of non-multidrug-resistant strain, only strains C and L were negative for both genes, whilst others were positive.

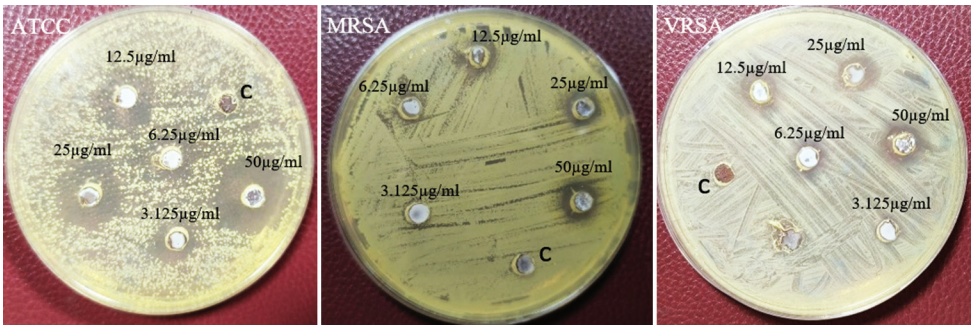

Fig. 5. The antibacterial action of different zinc oxide nanoparticles concentrations against *S. aureus* strains, and C as control (Zinc oxide dehydrate stock).

and characterization of ZnO-NPs from ATCC 25923 were achieved to the best of our knowledge in this study, with reproducible physicochemical and antibacterial properties. The deposition of white precipitates was the first sign of nano production at pH 12, as in similar research using pH 11–12 (Abdulqodus, et al., 2025), but in another study using other genera of bacteria, like *Bacillus subtilis*, the optimum pH was 7.5 (Hamk, Akcay, and Avci, 2023), so it depended on capping agents and biogenic molecules. The production of white powder has also been reported by several studies (El-Masry, et al., 2022; Mongy and Shalaby, 2024). The UV-Vis spectrum of the ZnO-NPs sample displayed a deep peak at 351nm, as observed in other studies (Narayana et al., 2020; Mongy and Shalaby, 2024), peaks at 340 nm and 358 nm, which were characteristic of ZnO-NPs. The same range of absorption peaks was also reported in earlier investigations of the biosynthesis of ZnO-NPs using microorganisms (Mohd Yusof, et al., 2020). FTIR spectroscopy was used

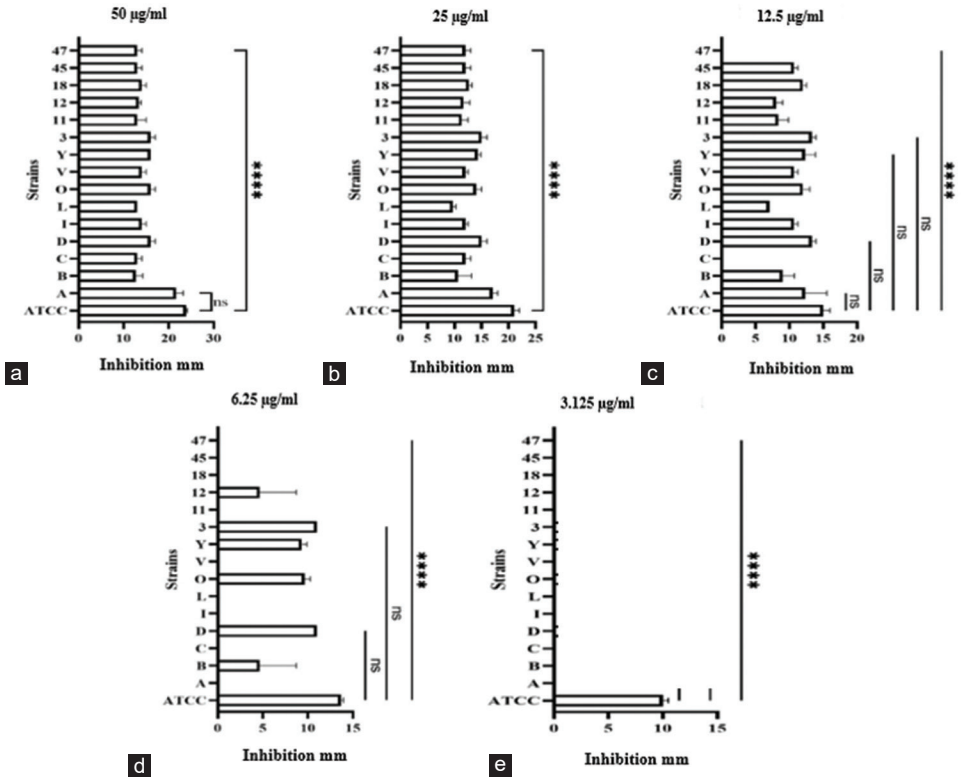

Fig. 6. (a-e) Histogram of the multicomparison test of antibacterial action of different concentrations (50, 25, 12.5, 6.25, and 3.125 µg/mL) of ZnO-NP between American Type Culture Collection and pathogenic strains. (ns) represent non-significant differences, and (****) represent statistical differences at $p<0.001$.

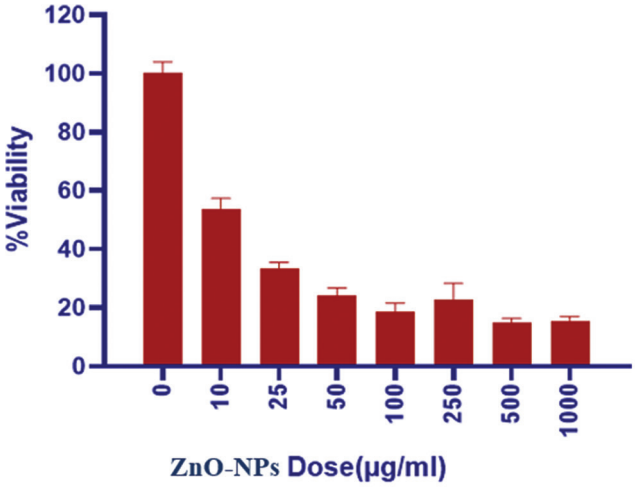

Fig. 7. Cytotoxicity effect of different concentrations of zinc oxide nanoparticles created by American Type Culture Collection (25923) by MTT assay against human embryonic kidney 293 cells, the IC_{50} was 14.8 µg/mL.

for evaluating the composition of bioactive molecules in ZnO-NPs for evaluating the stretching vibrations of Zn–O bonds, Proteins and carbohydrates were the source of this O-H group, found in bacterial supernatant, as the graph illustrates, and were thus in charge of the reduction and synthesis of ZnO-NPs, found in bacterial supernatant, as the graph illustrates, and were thus in charge of the reduction and synthesis of ZnO-NPs, as in other studies which were confirmed by the distinctive peaks at 618.95 cm^{-1} and 471 cm^{-1}, indicating the successful formation of ZnO NPs, which served as a core structure and were also supported by the results of the FTIR absorption spectra (Gangwar, et al., 2024) (Dhanalakshmi, Palanimurugan and Natarajan, 2018). The XRD pattern of ZnO-NPs showed strong, reproducible peaks, as mentioned by Epp (Epp, 2016). Understanding these corresponding planes was critical because it not only validates ZnO's crystalline phase and purity but also sheds light on the size, preferred orientation, and potential effects on functional properties of their crystallites. The most significant aspect of the result of the XRD pattern was the broad peaks (e.g., FWHM of 0.512° at location 36.059°). They did not indicate low-quality data; rather, they served as clear proof that you had created successful nanoscale crystals, similar to those reported (El-Masry, et al., 2022). Using electron microscopy, TEM, and FE-SEM to explain the NPs' size and shape. Our study reported that the particle size of ZnO-NPs, measured by TEM, was 48.8 ± 13.9 nm, and ranged from 20 to 50 nm. and FE-SEM were average diameters 74.7 ± 22.4nm, which were incompatible with Mohd Yusof, et al. developed ZnO NPs with irregular shapes (192 nm) and flower-like patterns (291 nm) (Mohd Yusof, et al., 2020), while Chakra, et al. reported a size range from 7 nm to 97 nm (Chakra, et al., 2025). The shape and size distribution were similar to other biofabricated ZnO morphologies, and the size distribution was aligned with other biosynthesized ZnO-NPs that were reported in recent studies. The mechanisms by which ZnO-NPs act as antimicrobials are not clear and

are under investigation; possibly the zinc+ ions generated by ZnO-NPs function as antimicrobial agents and antibiotics (Elbrolesy, et al., 2023). ZnO-NPs exhibit antibacterial effect against bacterial cell walls due to their tiny size and large area of surface (Taran, Rad and Alavi, 2018). Screening the *mecA* gene and *Int1*, which confer antibiotic resistance, found that ZnO-NPs delivered a significant inhibition concentration against both MRSA and VRSA strains. Most concentrations showed activity to inhibit bacterial growth in pathogenic strains; their effect was powerful against ATCC, which had an incredible capacity to develop antibiotic resistance, across all tested concentrations. Following additional research (Abdo, et al., 2021; El-Masry, et al., 2022) (Hamk, Akcay and Avci, 2023) (Elabbasy, et al., 2025), which mentions the antibacterial ability of ZnO-NPs against MDR strains, showed their potential to reduce bacterial infections (Taran, Rad and Alavi, 2018), in other study diameter zones were (17 mm in 100 μg/mL) (Sarwar, et al., 2025), 9–12 mm in 2000 μg/mL in (Elbrolesy, et al., 2023), and 13 mm in 1000 μg/mL (Khalid, et al., 2021) of ZnO-NPs against MDR strains was very high concentration when compared to the current study, which were (13–21 mm in 50 μg/mL) toward MDR strains, and also not anti-MRSA effect in (Abdelmigid, et al., 2022). Moreover, the result of the MTT assay showed the IC_{50} value, which was the inhibition concentration of ZnO-NPs that inhibits 50% of cell growth, was 14.8 μg/mL, due to the small size (48.8 ± 13.9 nm) of ZnO-NPs and their purity, as proven by different characterizations and also the relation between concentration of nano and viable cells but, other studies showed a bigger size of nano and a higher IC_{50}, like size 75–400 nm and IC_{50} 38.6 μg/mL (Perumal, et al., 2024), and size 118.6 nm and IC_{50} 111 μg/mL (Abdelmigid, et al., 2022).

IV. Conclusion

ZnO-NPs produced through green extracellular ATCC 25923 syntheses and the rate of biofabrication were significantly impacted by both pH and precursor concentration. At pH 12 with 4 mM $ZnSO_4 \cdot 7H_2O$, biosynthesis was high. ZnO-NPs had Average diameters of 48.8 ± 13.9 nm and were spherical crystalline in shape. The biosynthesis of ZnO-NPs and the stabilizing organic compounds were validated by EDS and FTIR analyses, respectively. Depending on this finding, ZnO-NPs biofabricated by bacteria were a powerful antibacterial agent against a variety of harmful strains, even against some MDR strains at 12.5 μg/mL and 6.125 μg/mL, but at the same time, they had cytotoxic effects, the IC_{50} was 14.8 μg/mL that may be significant, which encourages more researchers to standardize characterization and cytotoxicity methods for safer applications in biomedical and other fields.

References

Abdelmigid, H.M., Hussien, N.A., Alyamani, A.A., Morsi, M.M., AlSufyani, N.M., and Kadi, H.A., 2022. Green synthesis of zinc oxide nanoparticles using pomegranate fruit peel and solid coffee grounds vs. chemical method of synthesis, with their biocompatibility and antibacterial properties investigation. *Molecules*, 27(4), p.17.

Abdo, A.M., Fouda, A., Eid, A.M., Fahmy, N.M., Elsayed, A.M., Khalil, A.M.A., Alzahrani, O. M., Ahmed, A.F., and Soliman, A.M., 2021. Green synthesis of zinc oxide nanoparticles (zno-nps) by *Pseudomonas aeruginosa* and their activity against pathogenic microbes and common house Mosquito, *Culex pipiens*. *Materials (Basel)*, 14(22), p.16.

Abdulqodus, A.N., Abdulrahman, A.F., Mostafa, S.H., Kareem, A.A., Hamad, S.M., Ahmed, S.M., Almessiere, M.A., and Shaikhah, D., 2025. Green synthesis of ZnO nanoparticles: Effect of pH on morphology and photocatalytic degradation efficiency. *Applied Physics A*, 131(9), p.720.

Ali, K.M., and Al-Jaff, B.M.A., 2021. A Study on the Prevalence and Source of Staphylococci and methicillin-resistant *Staphylococcus aureus* causing superficial incisional surgical site infection. *Aro-the Scientific Journal of Koya University*, 9(1), pp.114-121.

Al-Naqshbandi, A.A., Hassan, H.A., Chawsheen, M.A., and Abdul Qader, H.H., 2021. Categorization of bacterial pathogens present in infected wounds and their antibiotic resistance profile recovered from patients attending Rizgary hospital-Erbil. *Aro the Scientific Journal of Koya University*, 9(2), pp.64-70.

Alnuaimi, M.T., Al-Janabi, Z.Z., Adel, M.M., and Alfahad, M.A., 2022. New trend on antimicrobial activity of green AgNPs from Trogoderma granarium larval extract against antibiotic-resistant *Salmonella* Typhi. *Egyptian Journal of Chemistry*, 66(6), pp.31-39.

Belteky, P., Ronavari, A., Zakupszky, D., Boka, E., Igaz, N., Szerencses, B., Pfeiffer, I., Vagvolgyi, C., Kiricsi, M., and Konya, Z., 2021. Are smaller nanoparticles always better? understanding the biological effect of size-dependent silver nanoparticle aggregation under biorelevant conditions. *International Journal Nanomedicine*, 16, pp.3021-3040.

Chakra, P.S., Banakar, A., Puranik, S.N., Kaveeshwar, V., Ravikumar, C.R., and Gayathri, D. 2025. Characterization of ZnO nanoparticles synthesized using probiotic *Lactiplantibacillus plantarum* GP258. *Beilstein Journal Nanotechnol*, 16, pp.78-89.

Dhanalakshmi, A., Palanimurugan, A., and Natarajan, B., 2018. Efficacy of saccharides bio-template on structural, morphological, optical and antibacterial property of ZnO nanoparticles. *Material Science Engineering C Material Biological Applications*, 90, pp.95-103.

Elabbasy, M.T., El Bayomi, R.M., Abdelkarim, E.A., Hafez, A.E.E., Othman, M.S., Ghoniem, M.E., Samak, M.A., Alshammari, M.H., Almarshadi, F.A., Elsamahy, T., and Hussein, M.A., 2025. Harnessing *Stevia rebaudiana* for Zinc oxide nanoparticle green synthesis: A sustainable solution to combat multidrug-resistant bacterial pathogens. *Nanomaterials (Basel)*, 15(5), p.369.

Elbrolesy, A., Abdou, Y., Elhussiny, F.A., and Morsy, R., 2023. Novel green synthesis of UV-sunscreen ZnO nanoparticles using *Solanum lycopersicum* fruit extract and evaluation of their antibacterial and anticancer activity. *Journal of Inorganic and Organometallic Polymers and Materials*, 33(12), pp.3750-3759.

El-Masry, R.M., Talat, D., Hassoubah, S.A., Zabermawi, N.M., Eleiwa, N.Z., Sherif, R.M., Abourehab, M.A.S., Abdel-Sattar, R.M., Gamal, M., Ibrahim, M.S., and Elbestawy, A., 2022. Evaluation of the antimicrobial activity of ZnO nanoparticles against enterotoxigenic *Staphylococcus aureus*. *Life (Basel)*, 12(10), p.1662.

Epp, J., 2016. X-ray diffraction (XRD) techniques for materials characterization. In: *Materials Characterization Using Nondestructive Evaluation (NDE) Methods.* United Kingdom, Woodhead Publishing, pp.81-124.

Fakhari, S., Jamzad, M., and Kabiri Fard, H., 2019. Green synthesis of zinc oxide nanoparticles: A comparison. *Green Chemistry Letters and Reviews*, 12(1), pp.19-24.

Gangwar, J., Balasubramanian, B., Pratap Singh, A., Meyyazhagan, A., Pappuswamy, M., Alanazi, A.M., Rengasamy, K.R.R., and Kadanthottu Sebastian, J., 2024. Biosynthesis of zinc oxide nanoparticles mediated by *Strobilanthes hamiltoniana*: Characterizations, and its biological applications. *Kuwait Journal of Science*, 51(1), p.100102.

Haji, S.H., Ali, F.A., and Aka, S.T.H., 2022. Synergistic antibacterial activity of silver nanoparticles biosynthesized by carbapenem-resistant Gram-negative bacilli. *Scientific Reports*, 12(1), p.15254.

Hamad, A.H., Chawsheen, M.A., and Al-Naqshbandi, A.A., 2022. Role of laser produced silver nanoparticles in reversing antibiotic resistance in some multidrugresistant pathogenic bacteria. *Aro the Scientific Journal of Koya University*, 10(1), pp.104-110.

Hamk, M., Akcay, F.A., and Avci, A., 2023. Green synthesis of zinc oxide nanoparticles using *Bacillus subtilis* ZBP4 and their antibacterial potential against foodborne pathogens. *Preparative Biochemistry Biotechnology*, 53(3), pp.255-264.

Hayat, S., Ashraf, A., Zubair, M., Aslam, B., Siddique, M.H., Khurshid, M., Saqalein, M., Khan, A.M., Almatroudi, A., Naeem, Z., and Muzammil, S., 2022. Biofabrication of ZnO nanoparticles using *Acacia arabica* leaf extract and their antibiofilm and antioxidant potential against foodborne pathogens. *PLoS One*, 17(1), p.e0259190.

Khalid, A., Ahmad, P., Alharthi, A.I., Muhammad, S., Khandaker, M.U., Faruque, M.R.I., Din, I.U., Alotaibi, M.A., and Khan, A., 2021. Synergistic effects of Cu-doped ZnO nanoantibiotic against gram-positive bacterial strains. *PLoS One*, 16(5), p.e0251082.

Mohd Yusof, H., Abdul Rahman, N.A., Mohamad, R., Zaidan, U.H., and Samsudin, A.A., 2020. Biosynthesis of zinc oxide nanoparticles by cell-biomass and supernatant of Lactobacillus plantarum TA4 and its antibacterial and biocompatibility properties. *Scientific Reports*, 10(1), p.19996.

Mohemmad, H.J., Abbas Alkhafaji, Y.A., and Alkafaji, H.R., 2023. Assessment of beta-lactamases and integrons genes among bacteria isolated from bladder cancer patients with urinary tract infections. *Journal of Population Therapeutics and Clinical Pharmacology*, 30(8), pp.e9-e23.

Mongy, Y., and Shalaby, T., 2024. Green synthesis of zinc oxide nanoparticles using Rhus coriaria extract and their anticancer activity against triple-negative breast cancer cells. *Scientific Reports*, 14(1), p.13470.

Narayana, A., Bhat, S.A., Fathima, A., Lokesh, S.V., Surya, S.G. and Yelamaggad, C.V. 2020. Green and low-cost synthesis of zinc oxide nanoparticles and their application in transistor-based carbon monoxide sensing. *RSC Advances*, 10, pp.13532-13542.

Omer, S.A., Ganjo, A.R., Haji, S.H., and Smail, S.B., 2024. Accessory gene regulator (agr) group polymorphisms in methicillin-resistant staphylococcus aureus and its association with biofilm formation. *Cellular and Molecular Biology (Noisy-le-grand)*, 70(4), pp.1-7.

Perumal, P., Sathakkathulla, N.A., Kumaran, K., Ravikumar, R., Selvaraj, J.J., Nagendran, V., Gurusamy, M., Shaik, N., Gnanavadivel Prabhakaran, S., Suruli Palanichamy, V., Ganesan, V., Thiraviam, P.P., Gunalan, S., and Rathinasamy, S., 2024. Green synthesis of zinc oxide nanoparticles using aqueous extract of shilajit and their anticancer activity against HeLa cells. *Scientific Reports*, 14(1), p.2204.

Rafael, B.F., Rodrigues, J.D., Lemos Barbosa, T.W., Goncalves Garcia, A.D., Porta, F.D.A.L., Pratavieira, S., Chiavacci, L.A., Araújo Junior, J.P., Da Costa, P.I., and Martinez, L.R., 2023. Zinc-Based Nanoparticles Reduce Bacterial Biofilm Formation. *Microbiology Spectrum*, 11(2), p.e0483122.

Sarwar, K., Nazli, Z.I.H., Munir, H., Aslam, M., and Khalofah, A., 2025. Biosynthesis of zinc oxide nanoparticles using *Moringa oleifera* leaf extract, probing antibacterial and antioxidant activities. *Scientific Reports*, 15, p.20413.

Taran, M., Rad, M., and Alavi, M., 2018. Biosynthesis of TiO2 and ZnO nanoparticles by *Halomonas elongata* IBRC-M 10214 in different conditions of medium. *Bioimpacts*, 8(2), pp.81-89.

Wei, J., Ma, K., Zhang, Y., Yang, X., Tang, Q., and Nie, Z., 2023. Correlation analysis of *Staphylococcus aureus* drug resistance and virulence factors with blood cell counts and coagulation indexes. *International Journal of Clinical Practice*, 2023, p.8768152.